Research Paper

STARD1 and NPC1 expression as pathological markers associated with astrogliosis in post-mortem brains from patients with Alzheimer's disease and Down syndrome

Fabian Arenas[1,2], Fernanda Castro[1,2], Susana Nuñez[1,2], Gemma Gay[1], Carmen Garcia-Ruiz[1,2,3,4], Jose C. Fernandez-Checa[1,2,3,4]

[1]Department of Cell Death and Proliferation, Institute of Biomedical Research of Barcelona (IIBB), CSIC, Barcelona, Spain
[2]Liver Unit, Hospital Clinic I Provincial de Barcelona, Instituto de Investigaciones Biomédicas August Pi i Sunyer (IDIBAPS), Barcelona, Spain
[3]Centro de Investigación Biomédica en Red (CIBEREHD), Barcelona, Spain
[4]Research Center for ALPD, Keck School of Medicine, University of Southern California, Los Angeles, CA 90033, USA

Correspondence to: Jose C. Fernandez-Checa, Carmen Garcia-Ruiz; **email:** checa229@yahoo.com, cgrbam@iibb.csic.es
Keywords: cholesterol, NPC1, StARD1, mitochondria, lysosomes
Received: July 23, 2019 **Accepted:** December 23, 2019 **Published:** January 5, 2020

ABSTRACT

Alzheimer´s disease (AD) is a progressive neurodegenerative disorder of complex etiology, while Down syndrome (DS) is considered a genetically determined form of AD. Alterations in cholesterol homeostasis have been linked to AD although the role in this association is not well understood. Increased expression of STARD1 and NPC1, which are involved in intracellular cholesterol trafficking, has been reported in experimental AD models but not in patients with AD. Here we analyzed endolysosomal/mitochondrial cholesterol homeostasis, expression of NPC1 and STARD1 and correlation with pathological markers of AD in cortex and hippocampus from post-mortem brains from patients with AD and DS. NPC1 expression was observed in hippocampus from patients with AD and DS. Moreover, STARD1 expression increased in hippocampus and cortex from patients with AD and DS, respectively, and its immunoreactivity discriminated controls from AD or DS with a better accuracy than $A\beta_{42}$. Hippocampal areas stained with the recombinant GST-PFO probe showed increased mitochondrial cholesterol within astrocytes of brains from patients with AD and DS-brains compared to controls. Lysosomal cholesterol accumulation within hippocampal astrocytes was higher in DS than in AD. These data revealed increased intracellular cholesterol loading in hippocampus from patient with AD and DS and suggest that STARD1 could be a potential pre-clinical marker associated with early stages of AD pathology.

INTRODUCTION

Alzheimer's disease (AD) is a progressive neuro-degenerative disorder of complex etiology and the most common form of dementia, which comprises early-onset AD (EOAD, ~5% of patients) and late-onset AD (LOAD, 95% of patients). The generation of toxic beta amyloid (Aβ) peptides is considered a central player in AD patho-genesis, although other factors such as tau phosphorylation are also key for the progression of AD [1]. While alterations in cholesterol homeostasis have been linked to AD the role for this association is controversial. For instance, there has been evidence indicating that either increased or decreased total brain cholesterol levels are associated with AD-pathogenesis [2]. Whether intracellular cholesterol pools (e.g.

endolysosomes and mitochondria) rather than total cholesterol levels are more relevant for AD pathology remains to be established. Indeed, hippocampus and frontal cortex of patients with AD and AD-Tg mice have been shown to exhibit increased expression of the lysosomal cholesterol transporter NPC1 [3], while increased steroidogenic acute regulatory protein (STARD1) expression, which regulates the mitochondrial cholesterol trafficking [4], has been reported in pyramidal hippocampal neurons of patients with AD [5]. Moreover, mitochondrial cholesterol accumulation in a hyper-cholesterolemic AD-Tg mouse model has been shown to impair mitochondrial antioxidant defense and stimulate oxidative stress, which results in the acceleration of AD-like neuropathology [6, 7]. However, the intracellular cholesterol homeostasis in human AD has not been explored.

Down syndrome (DS) is considered a genetically determined form of AD and individuals with DS invariably develop AD by their fourth decade [8]. Patients with DS exhibit cognitive markers of preclinical and prodromal AD [9]. The progression of AD pathology assessed by neuroimaging and/or cerebrospinal fluid levels of Aβ and tau (total and phosphorylated) revealed a similar pattern between normal population and individuals with DS, although these events in DS occur 10–20 years earlier than in normal population [10, 11]. Aging, obesity and ApoEε4-associated dyslipidaemia are important risk factors for development of AD dementia in normal and DS population [12]. Interestingly, hypercholesterolemic subjects with DS treated with statins exhibit a lower risk factor for AD development that correlates with slower amyloidogenic burden [13]. Besides the overlap between AD and DS, intracellular brain cholesterol homeostasis in patients with DS has not been reported. We hypothesized that alterations in intracellular cholesterol homeostasis in lysosomes and mitochondria in the brain could contribute to the molecular events involved in the AD *continuum*, emerging as a pathological event that could contribute to disease progression. Investigating the intracellular cholesterol homeostasis is critical to improve and expand the therapeutic armamentarium for AD, especially at preclinical stages, given that current clinical trials for AD have been disappointing. In contrast to the controversial role of changes in total brain cholesterol levels in AD [2, 14], our findings on the expression of putative intracellular cholesterol carriers (e.g. STARD1 and NPC1) in patients with AD and DS correlate with disease markers, such as $A\beta_{42}$, and suggest that alterations in intracellular cholesterol homeostasis may be an early molecular event that favours the progression of the AD pathology. Moreover, the accuracy of STARD1 to discriminate controls from AD in the general population and in subjects with DS suggests that StARD1 could be a potential novel marker associated with early molecular events of AD pathology in both populations.

RESULTS

Intracellular cholesterol homeostasis in cortex from patients with AD and DS

As alterations in cortex occur late in AD and reflect disease progression, we first examined the intracellular cholesterol homeostasis in the cortex of sporadic AD and DS using post-mortem cryopreserved cortex samples from patients with AD and DS (Table 1). Transcripts and protein expression of putative cholesterol carriers involved in intracellular cholesterol trafficking (NPC1, STARD3/MLN64, STARD4, and STARD1), as well as sensors/regulators of *de novo* cholesterol synthesis (INSIG-1 and SREBP2) were examined [2] and summarized in Supplementary Table 1. While the expression at mRNA or protein levels of STARD4, INSIG-1 and mature SREBP2 (mSREBP2) seems to be similar between AD, DS and control samples (Figure 1), cortex from patients with DS exhibited a significant overexpression of transcripts for the mitochondrial carrier STARD1 (Figure 1A), which translated at the protein levels (Figure 1B). Moreover, there was a trend for increased mRNA levels of NPC1 and STARD3/MLN64 in cortex from patients with DS (Figure 1A). In addition, cortex from AD-brains exhibited a small but significant increase in the NPC1 protein expression compared to control samples and a trend for increased STARD1 protein levels (Figure 1B). These findings indicate that cortex from patients with DS and AD exhibit increased expression of StARD1 and NPC1, respectively.

STARD1 and NPC1 immunoreactivity in hippocampus from patients with AD and DS

AD pathology is characterized by atrophy in hippocampus, temporal lobes and parietotemporal cortices where neuronal death correlates with amyloid plaques (largely composed of $A\beta_{42}$) and neurofibrillary tangles (NFTs) [15]. Interestingly, an accelerated Aβ burden with greater plaques deposition and NFT have been described in the hippocampus of DS subjects exhibiting AD pathology [8]. Therefore, we examined the hippocampal expression of cholesterol carriers involved in lysosomal (i.e. NPC1) and mitochondrial (i.e. STARD1) trafficking and compared this outcome with the pathological markers $A\beta_{42}$ and p-tau, summarized in Supplementary Table 1. Immuno-histochemical analysis of paraffin-fixed hippocampal sections showed increased $A\beta_{42}$ and p-tau

Table 1. Collected specimens from cases of AD, DS and controls.

	Subjects (males/females)						
Group	**Cryopreserved Cortex**	**Paraffined hippocampus**	**Cryopreserved hippocampus**	**Total subjects**	**Mean age ± SEM**	**Anatomopatho-logic diagnosis**	**Clinical diagnosis**
DS	5 (3/2)	7 (3/4)	4 (2/2)	7 (3/4)	56 ± 4.31	AD V-VI, CERAD C	Dementia
AD	5 (2/3)	7 (4/3)	5 (2/3)	7 (4/3)	80.7 ± 3.00	AD V-VI, CERAD B-C	Dementia
Control	6 (4/2)	7 (5/2)	5 (4/1)	7 (5/2)	69.7 ± 4.79	Without neurological lesions (5)	Cognitively healthy
						Frontotemporal degeneration (1)	FTD
						iLBD; incidental Lewy body disease (1)	Cognitively healthy

Note: For immunohistochemical and immunofluorescence analysis, 5 µm thin paraffin sections of hippocampus were available for all human brain samples, while 14 µm thin sections of frozen hippocampus were available for just 19 cases to analyse the intracellular cholesterol levels by immunofluorescence. On the other hand, cryopreserved human cortex of just 16 donors were available to assess gene expression and western blotting analysis. FTD, frontotemporal dementia.

immunoreactivity in patients with AD and DS compared with control subjects (arrows in Figure 2A and 2B). These differences were significant for $A\beta_{42}$ staining in CA1, CA2 and CA3 hippocampal regions from patients with DS, in agreement with the intrinsic overproduction of Aβ in this population [8]. Moreover, there was a trend for increased $A\beta_{42}$ in CA1 region from patients with AD. Interestingly, CA1, CA2 and CA3 hippocampal regions from patients with AD and DS showed a significant higher NPC1 protein expression than control samples (Figure 2A and 2B). In line with previous findings [5], the expression of StARD1 in hippocampal regions revealed a significant increase of STARD1 immunoreactivity in CA1 and CA3 areas from patients with AD compared with DS and controls (Figure 2A and 2B). Moreover, when STARD1 and $A\beta_{42}$ immunoreactivity were compared among all samples, the hippocampal region-specific pattern of STARD1 expression significantly correlated with $A\beta_{42}$ deposition in CA1 and CA3 (Figure 2C). Thus, although AD and DS are two related diseases, each exhibit specific changes regarding the expression of intracellular cholesterol carriers STARD1 and NPC1, with STARD1 overexpression in hippocampus being specific for AD while in cortex the increase seems to be characteristic of DS. In contrast, the increase in expression of NPC1 occurs in both diseases. In addition, the differential turnover between proteins and their corresponding mRNA likely contribute to the specific pattern of expression of STARD1 and NPC1 at the mRNA and protein levels in the cortex between AD and DS samples. Further research will be required to understand the full impact of these changes in AD pathology and its genetically related form DS.

Discrimination capacity of NPC1 and STARD1 immunoreactivity in hippocampus from patients with AD and DS

In analogy with $A\beta_{42}$, we searched for expression of both NPC1 and STARD1 in the paraffin-fixed hippocampal samples as potential discrimination factors between AD and/or DS from normal controls. For each hippocampal region we analyzed the relative area immunolabeled with $A\beta_{42}$, NPC1, and STARD1 and performed ROC curves analysis between controls subjects and patients with AD, DS, or the sum of both AD+DS groups (Figure 3). As expected, $A\beta_{42}$ deposition revealed a highly significant AUC with a high accuracy not only to identify AD and/or DS samples as positive (sensitivity), particularly in CA1 hippocampal areas, but also to identify the control subjects (specificity) in all hippocampal regions from DS-brains (Figure 3). Similarly, in hippocampal CA1 and CA3 regions, NPC1 immunolabeling properly discriminated AD individuals, but not DS subjects, from controls (Figure 3). Unexpectedly, STARD1 discriminated AD and/or DS samples from control individuals in all hippocampal regions (Figure 3), suggesting that STARD1 immunolabeling exhibits a greater discrimination capacity than $A\beta_{42}$. Moreover, multivariate data analysis of the cohort by principal components analysis (PCA) showed an efficient

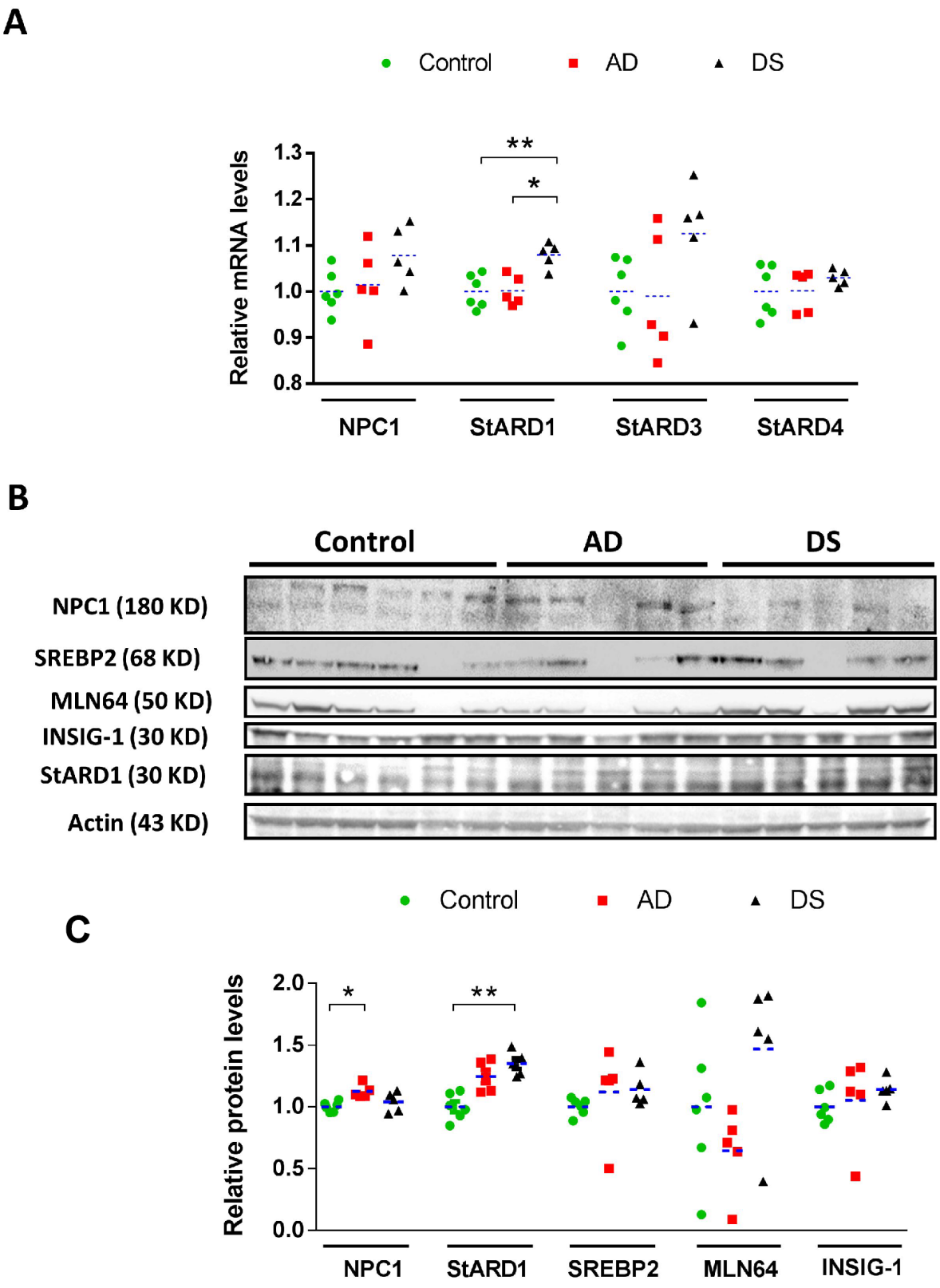

Figure 1. Cortical expression profile of intracellular cholesterol carriers and sensors/regulators. (**A**) Relative mRNA levels of NPC1, StARD3, StARD4, and StARD1 in human cortex from AD (n=5), DS (n=5), and control (n=6) subjects. Transcripts levels were normalized with respect to controls using β-actin. (*) p<0.05; (**) p<0.01. (**B**) Immunoblotting of NPC1, StARD1, StARD3/MLN64, mSREBP2 and INSIG-1 of total protein extracts (90 µg/lane) from human cortex from AD (n=5), DS (n=5), and control (n=6) donors. (**C**) Protein levels quantified by densitometry and normalized using β–actin as housekeeping followed by normalization with control group. (*) p<0.05; (**) p<0.01.

visualization of the data for CA1 and CA3, capturing more than 97.6% and 85% of the markers variability, respectively, with a clear separation between control subjects from AD and DS patients (Supplementary Figure 1).

Amyloid-related hippocampal astrogliosis associated with increased lysosomal and mitochondrial cholesterol content in patients with AD and DS

To investigate whether disruption of intracellular cholesterol homeostasis correlate with AD, we used confocal immunofluorescence imaging to explore the pattern distribution of the intracellular cholesterol transporters NPC1 and STARD1 within the astrocytes surrounding amyloid deposition in the different hippocampal regions (Figure 4). In agreement with previous observations in post-mortem human AD tissues as well as in animal models [16, 17], reactive astrocytes surrounding $A\beta_{42}$ deposition were observed in hippocampus from patients with AD and DS (Figure 4A). Moreover, the colocalization analysis of ten representative images per sample revealed that astrocytes in hippocampus from patients with DS

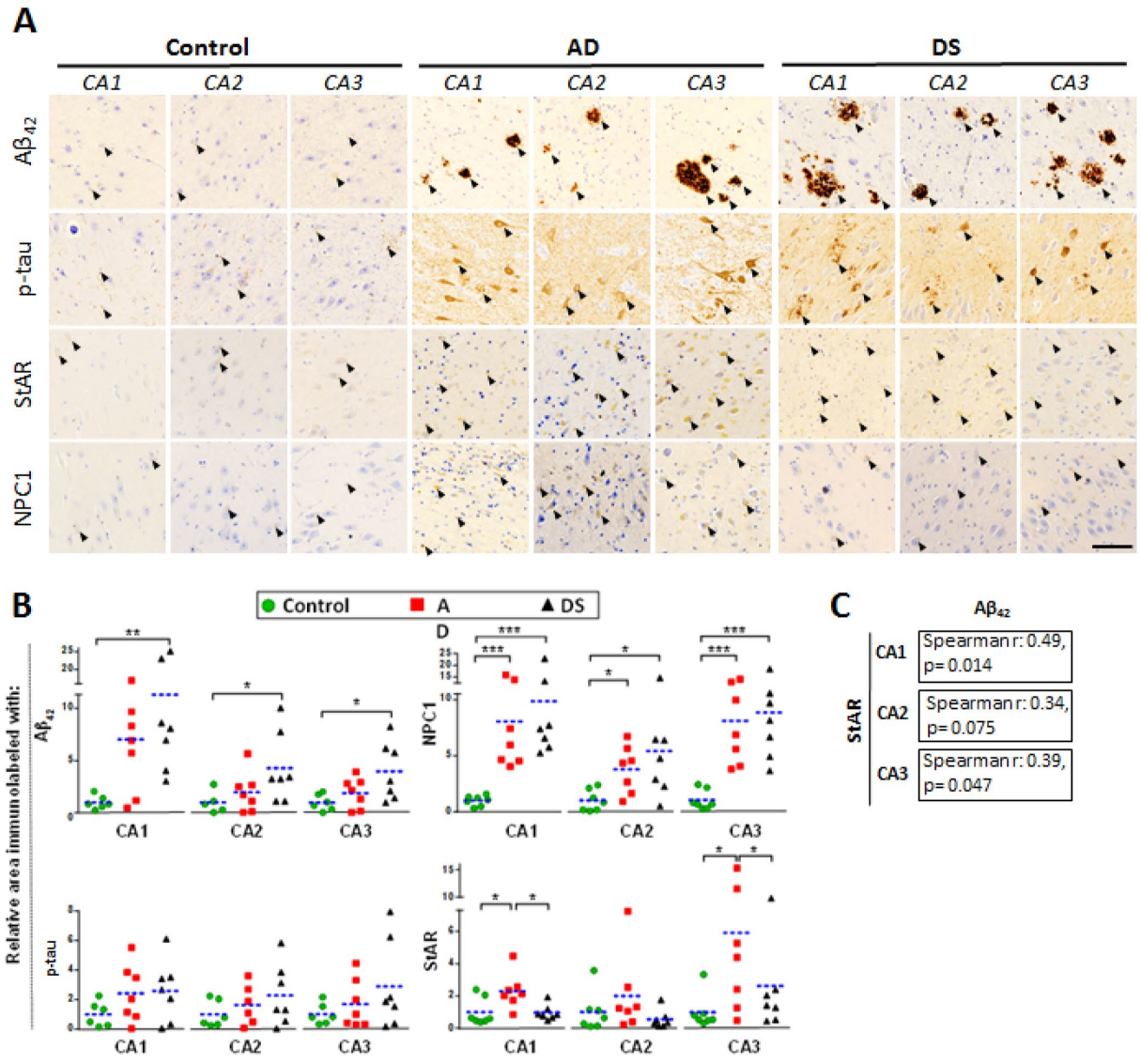

Figure 2. Hippocampal expression of AD biomarkers and lysosomal/mitochondrial cholesterol carriers. (**A**) Representative images of immunohistochemistry of paraffin sections (5 µm) against $A\beta_{42}$, p-tau, StARD1 and NPC1 for CA1, CA2 and CA3 hippocampal regions from AD (n=7), DS (n=7), and control (n=7) subjects. Positive immunoreactivity is shown by black arrows. Scale bar: 100 µm. (**B**) Quantitation of IHC shown in A using Image J software as described in Supplementary methods. For each hippocampal region, the % of immunolabeled area was normalized to control group. (*) p<0.05; (**) p<0.01; (***) p<0.001. (**C**) Spearman's correlation values between IHC-immunolabeling for $A\beta_{42}$ and StARD1 in each hippocampal region.

exhibit higher NPC1 expression than in AD and control samples, particularly in CA3 region (Figure 4B), suggesting increased lysosomal cholesterol levels in astrocytes from patients with DS. In addition, the analysis of the STARD1 content in hippocampal astrocytes indicated a region-specific significant increase of STARD1/GFAP colocalization index in CA1 and CA3 areas for patients with AD and DS, respectively, compared to controls (Figure 4B). Moreover, pilot observations following the staining of

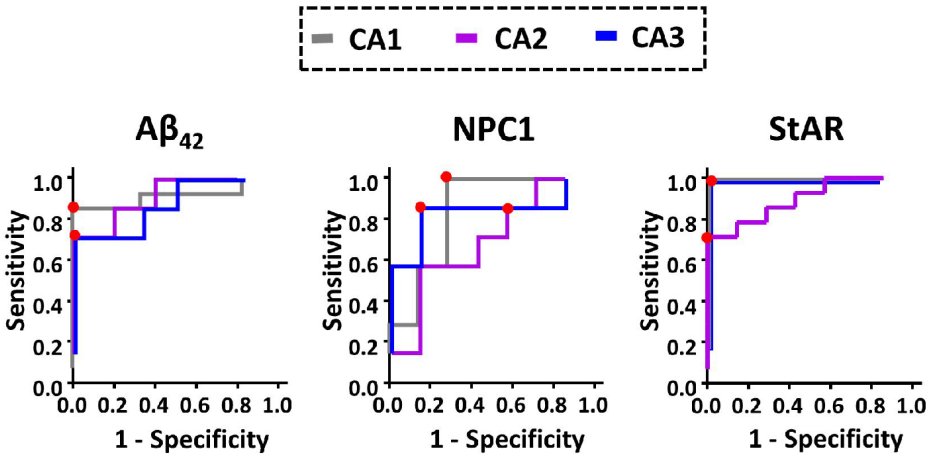

CA1

Ctrl *vs.*	AD+DS			AD			DS		
	Aβ42	*StAR*	*NPC1*	*Aβ42*	*StAR*	*NPC1*	*Aβ42*	*StAR*	*NPC1*
AUC	0.92	1.00	0.76	0.83	1.00	0.84	1.00	1.00	0.66
p	*	**	ns	*	**	*	**	**	ns
Specificity	1.00	1.00	0.71	1.00	1.00	0.57	1.00	1.00	0.71
Sensitivity	0.86	1.00	0.93	0.71	1.00	1.00	1.00	1.00	0.86
Accuracy	0.88	1.00	0.89	0.82	1.00	0.89	0.88	1.00	0.91

CA2

Ctrl *vs.*	AD+DS			AD			DS		
	Aβ42	*StAR*	*NPC1*	*Aβ42*	*StAR*	*NPC1*	*Aβ42*	*StAR*	*NPC1*
AUC	0.76	0.90	0.57	0.60	0.90	0.69	1.00	0.90	0.56
p	ns	*	ns	ns	*	ns	**	*	ns
Specificity	0.80	1.00	0.86	0.80	1.00	0.86	1.00	1.00	0.57
Sensitivity	0.71	0.71	0.36	0.57	0.71	0.57	1.00	0.71	0.71
Accuracy	0.71	0.83	0.46	0.68	0.83	0.46	0.88	0.83	0.49

CA3

Ctrl *vs.*	AD+DS			AD			DS		
	Aβ42	*StAR*	*NPC1*	*Aβ42*	*StAR*	*NPC1*	*Aβ42*	*StAR*	*NPC1*
AUC	0.80	1.00	0.78	0.71	1.00	0.84	0.88	1.00	0.70
p	*	***	*	ns	**	*	*	**	ns
Specificity	1.00	1.00	0.85	1.00	1.00	0.86	1.00	1.00	0.86
Sensitivity	0.64	1.00	0.79	0.57	1.00	0.86	0.71	1.00	0.71
Accuracy	0.71	1.00	0.80	0.71	1.00	0.80	0.71	1.00	0.80

Figure 3. Discrimination capacity of amyloid accumulation and lysosomal/mitochondrial cholesterol carriers. ROC curves of immunolabel for $A\beta_{42}$, NPC1, and StARD1 in each hippocampal region with the significantly highest AUC resulted in the comparison between control and AD, DS, or AD+DS groups (Lower panel). Red dots show the cutoff for the corresponding IHC-immunolabel that better discriminate AD and/or DS condition from normal controls in each hippocampal region. (*) $p<0.05$; (**) $p<0.01$; (***) $p<0.001$.

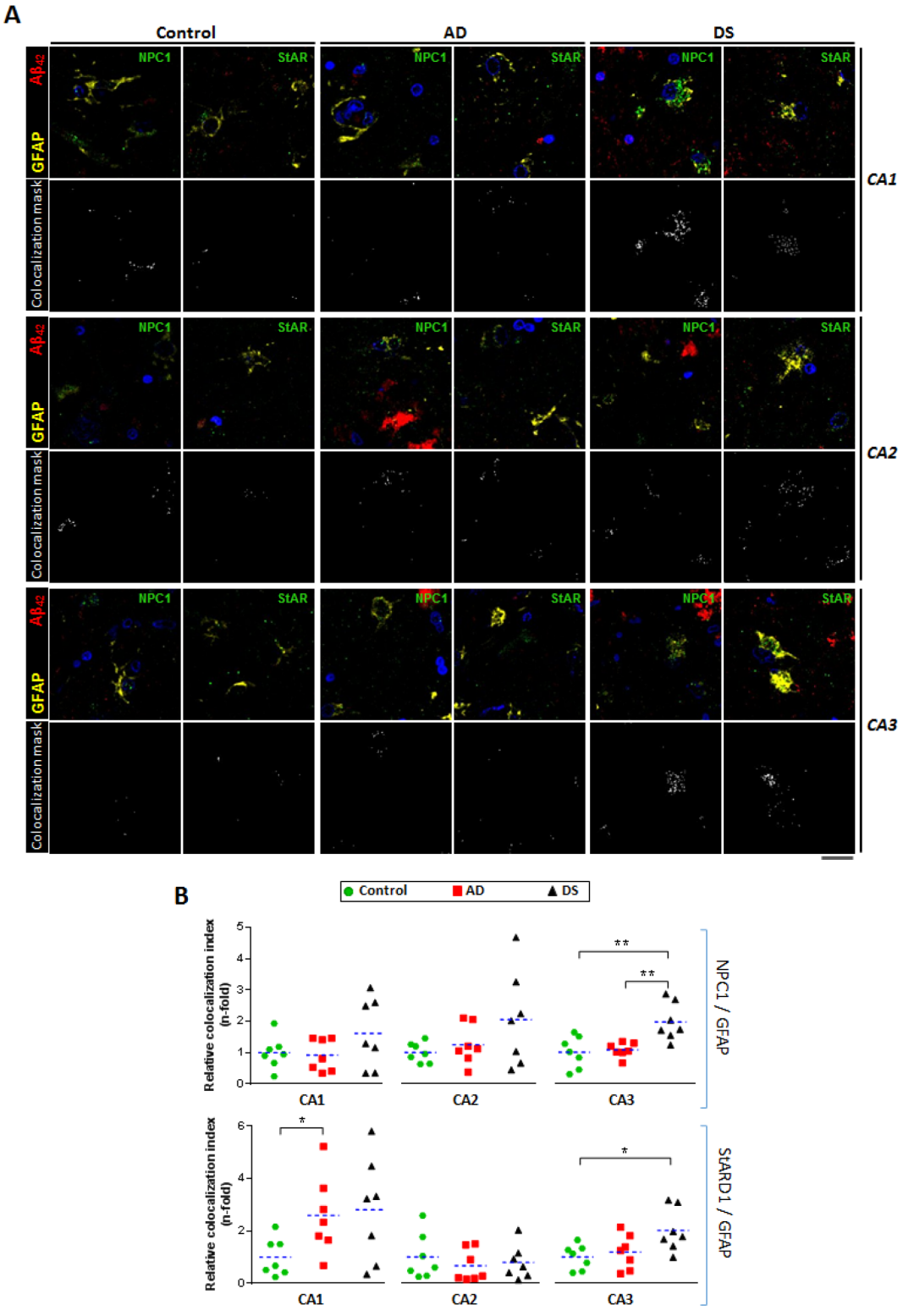

Figure 4. Astrocytes-expressing lysosomal and mitochondrial cholesterol carriers in hippocampal regions. (**A**) Representative confocal images of paraffined hippocampal regions (5 µm) from AD (n=7), DS (n=7), and control (n=7) subjects immunolabeled against $A\beta_{42}$ (red), GFAP (yellow), and NPC1 or StARD1 (both green). Nuclei are stained with Hoechst 33342 (blue). Lower panels show the colocalization mask between GFAP and NPC1 or StARD1 (white) highlighted in the squared areas. Scale bar: 10 µm. (**B**) Astrocyte colocalization with NPC1 (lysosomal) and StARD1 (mitochondrial) cholesterol carriers into hippocampal regions from AD, DS, and control subjects. 10 images per hippocampal region and per sample were analysed with Image J to assess the index of astrocyte (GFAP+) colocalization with NPC1 or StARD1. (*) p<0.05; (**) p<0.01; (***) p<0.001.

paraffined hippocampal sections of brains from AD, DS and control groups with NeuN and IBA1 antibodies as neuronal and glial markers, respectively, indicated that STARD1 and NPC1 expression increased in hippocampal neurons from AD and DA brains with respect to control, without changes in glia (not shown).

To assess the intracellular cholesterol distribution within hippocampal astrocytes (i.e. GFAP+), cryopreserved hippocampal samples of patients with AD and DS were analysed for the colocalization between GST-PFO probe, which detects cholesterol in membranes, with Lamp1 or Tom20 immunoreactivity to stain lysosome or mitochondria, respectively (Figure 5; and Supplementary Table 2). In line with the STARD1/GFAP colocalization, we found that the mitochondrial cholesterol content into hippocampal astroglia from patients with AD and DS was >2.5-fold higher than control donors (Figure 5B). Moreover, astroglial lysosomal cholesterol accumulation (PFO/Lamp1 in GFAP+) significantly increased in hippocampus from AD and DS patients compared to controls (Figure 5B), an outcome that was more pronounced in DS (14.41±1.322 fold) than in AD brains (3.43±0.502 fold). Interestingly, these findings correlated with the increased $A\beta_{42}$ accumulation in the CA1, CA2 and CA3 hippocampal regions of DS-brains (Figure 2B). Furthermore, PCA analysis revealed that the levels of astroglial NPC1 and STARD1 content as well as the intraorganelle-cholesterol levels are able to separate each group (Supplementary Figure 2).

DISCUSSION

We have analyzed the intracellular cholesterol trafficking in post-mortem samples from patients with DS and AD and assessed whether this event correlated with AD markers. An intriguing finding was that $A\beta_{42}$

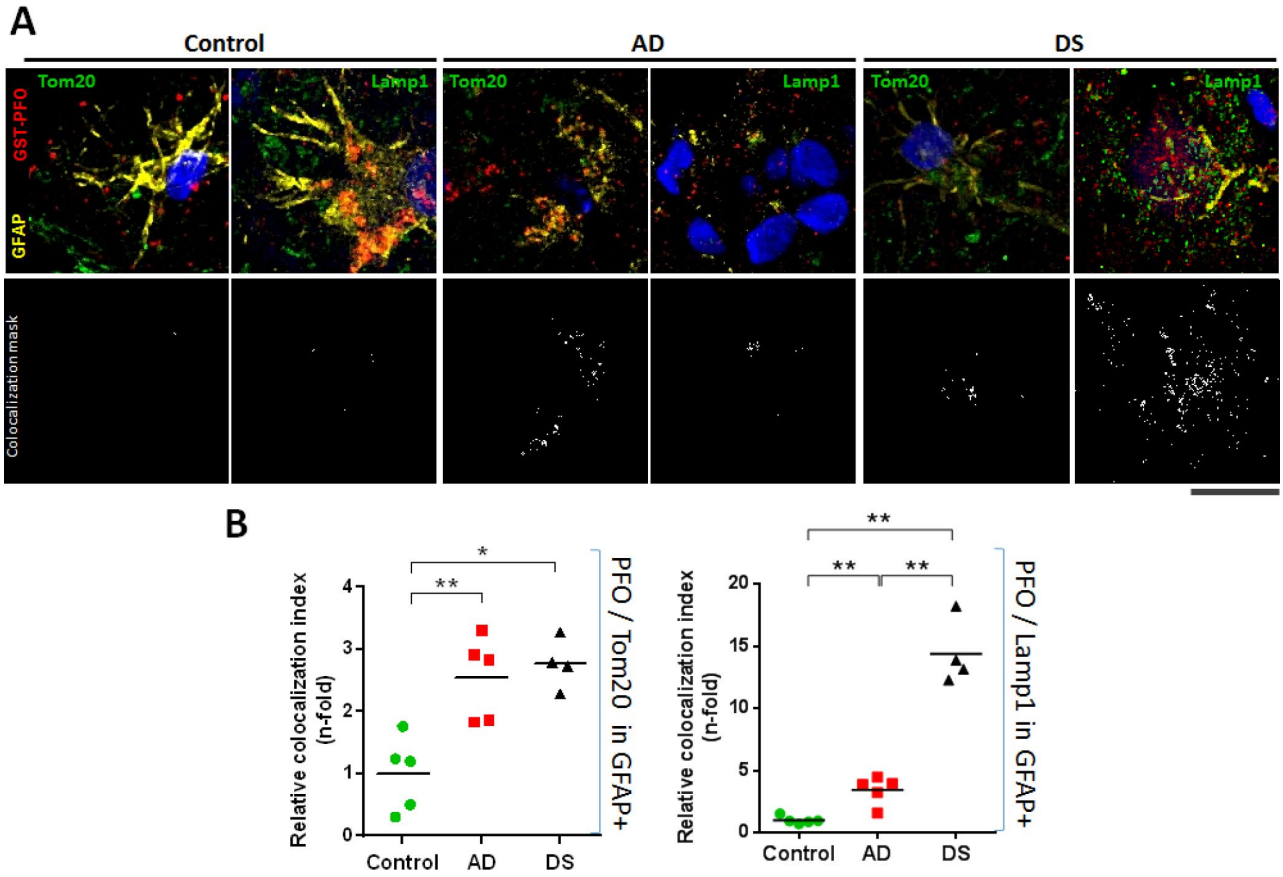

Figure 5. Lysosomal and mitochondrial cholesterol homeostasis in hippocampal astrocytes. (**A**) Representative confocal representative images of 4 µm thin-stacked cryopreserved hippocampus from AD (n=5), DS (n=4), and control (n=5) subjects immunolabeled with GST-PFO (red), GFAP (yellow), and Tom20 or Lamp1 (both green). Nuclei are stained with Dapi (blue). Lower panels show colocalization mask (white) between GST-PFO and Tom20 or Lamp1, respectively, highlighted in the squared areas. Scale bar: 10 µm. (**B**) Cholesterol (PFO+) colocalization with mitochondria (Tom20+) or lysosome (Lamp1+) into hippocampal astrocytes (GFAP+) from AD, DS, and control donors. 10 images per sample were analysed with Image J to assess the index of astrocytic cholesterol colocalization with Tom20 or Lamp1. Values are relativized with control to show differences as n-fold. (*) $p<0.05$; (**) $p<0.01$.

but not p-tau immunoreactivity significantly increased in CA1-3 hippocampal regions only in patients with DS, with a trend for increased $A\beta_{42}$ levels in CA1 from patients with AD. These findings in DS are consistent with the intrinsic Aβ overproduction in these subjects [8]. Moreover, neuropathological analysis of amyloid pathology in DS described the onset of mid-severity changes in hippocampal CA1 region at 35 years of age, in which $A\beta_{42}$ deposition occurred in the absence of tau pathology [18]. Conversely, tauopathies and the presence of NFTs that commonly coexist with LOAD can occur without amyloid pathology [19, 20]. In addition, it has been suggested that the earliest appearance of tau pathology in AD occurs in the *locus caeruleus* instead of hippocampus [21], which could account for the lack of p-tau immnunoreactivity in hippocampal samples from our cohort of patients with AD. While the present work is the first to our knowledge to address the expression of putative intracellular cholesterol carriers (e.g. STARD1 and NPC1) in AD and DS and their correlation with pathological markers, the role of changes in total cholesterol levels in AD is controversial [2, 14], consistent with the unsettled impact of statins in the prevention or treatment of the disease, which will require further randomized controlled trials [22, 23].

Although the groups studied were not age-matched given the limited number of samples and the life-expectancy of individuals with DS [8], we performed the comparisons with AD and controls considering AD pathogenesis as a function of age in DS, a population that exhibit a high risk to develop AD-type dementia [12, 24]. Moreover, as described previously [18], individuals with DS developed signs of AD-pathology by 50-55 years of age, which coincides with the age range of the subjects with DS analyzed in our study (Table 1). In this context, interestingly we found increased expression of NPC1 and STARD1 in cortical samples from patients with AD and DS, respectively, (Figure 1). A link between lysosomal cholesterol and $A\beta_{42}$ deposition in neurodegeneration has been described in Niemann–Pick type C (NPC) disease, a rare autosomal recessive disease associated mostly with NPC1 mutations, characterized by lysosomal accumulation of unesterified cholesterol [25]. While the etiology and epidemiology of AD and NPC differ, these neurodegenerative diseases share many disease-related molecular pathways, including cholesterol accumulation, lysosomal abnormalities, tau hyperphosphorylation, APP processing and Aβ deposition [2, 25]. Moreover, while increased mRNA and protein levels of NPC1 have been described within the hippocampus of both patients with AD and mice [3], the hippocampal expression pattern of NPC1 in human DS-brains has not been reported. Our findings suggest that while altered hippocampal NPC1 expression could be a common feature of DS and AD (Figure 2), the NPC1 immunolabeling as a disease marker of AD does not discriminate AD-pathology in patients with DS from the controls (Figure 3), suggesting that the AD *continuum* in the hippocampus of subjects with DS differs from NPC disease.

Cholesterol is known to promote the amyloidogenic processing of APP, which occurs predominantly in lipid-rafts where most components of the amyloidogenic machinery, such as APP, Aβ, BACE1, presenilins (PSEN1/2), and γ-secretase are present [26, 27]. Moreover, cholesterol is thought to interfere with the α-secretase-dependent non-amyloidogenic APP processing [28], and PSEN1/2 and γ-secretase have been localized at the mitochondrial ER-associated membrane (MAM) [29, 30]. Interestingly, although mitochondrial membranes are low in cholesterol, the pool of cholesterol of the mitochondrial inner membrane (MIM) is crucial for the synthesis of neurosteroids to maintain physiological GABAergic responses that modulate memory function, which is particularly affected in subjects with DS [31, 32]. The STARD1-dependent trafficking of cholesterol to MIM is the rate-limiting step for steroidogenesis and changes in mitochondrial cholesterol levels can impact this process and affect mitochondrial antioxidant defense [2, 5–7, 33]. However, the role of STARD1 in human AD is poorly understood and has not been examined in DS. We show for the first time that the hippocampal overexpression of STARD1 correlates with amyloid deposition suggesting a relationship between the accumulation of mitochondrial cholesterol and the development of AD-pathology (Figure 2). Unexpectedly, our findings in hippocampal samples from patients with DS and AD suggest that STARD1 immunolabeling can act as a pathological mark of AD even better than $A\beta_{42}$ deposition in post-morten samples (Figure 3), implying that the hippocampal alterations in the expression of STARD1 could occur in a temporal pattern parallel to the pathogenic amyloidogenic burden. Whether these alterations in STARD1 occur before $A\beta_{42}$ deposition in human AD requires further investigation. However, previous evidence in experimental models pointed that enhanced mitochondrial cholesterol levels in AD mouse models have been shown to sensitize neurons to Aβ-induced inflammation and toxicity by depleting mGSH by an ER stress-dependent mechanism [6, 7, 33]. Moreover, as Aβ-induced ER stress is considered an indirect effector of the Aβ-neurotoxicity in early stages of AD [34], our data suggest that STARD1 overexpression in the hippocampus may be a potential early molecular event associated with AD, as strengthened by the increase seen in DS, an accelerated genetic form of AD. In this context, it is widely recognized that neuro-inflammation in AD is an early pathological-associated response, which is exacerbated with ageing and contributes to disease progression [18, 35].

Although not statistical significant, our findings do suggest a trend for lower expression of STARD3/MLN64 in the cortex of AD samples (Figure 1B), whose impact in regulating the mitochondrial pool of cholesterol remains to be understood. In this regard, it is interesting to note that increased expression of MLN64 has been reported in the lysosomal storage disorder Niemann-Pick type C disease, which correlated with increased mitochondrial cholesterol accumulation [36]. However, it has also been reported that targeted mutations of the MLN64 START domain have been shown to cause minor alterations in metabolism and intracellular distribution of cholesterol [37]. Further investigation will be required to decipher the impact of MLN64 in mitochondrial cholesterol regulation and AD pathogenesis.

Reactive astrogliosis has emerged as a relevant pathological response in the early stages of AD [38], which correlates with cognitive decline [16]. Since astrocytes are the most prevalent cell type in the brain and form an intricate system of connections to control a wide range of brain functions, including regulation of blood-brain barrier, the astroglial atrophy could have far-reaching consequences on synaptic transmission that accounts for the spatio-temporal progression of AD-neurodegeneration [17]. We confirm the presence of reactive astrocytes surrounding amyloid plaque in the hippocampus of AD and DS, and observed a hippo-campal region-specific increased expression of STARD1 within astocytes (Figure 4) that correlates with the accumulation of mitochondrial cholesterol in both groups (Figure 5). Similarly, we also found astroglial NPC1 overexpression and astroglial accumulation of lysosomal cholesterol in AD and DS (Figures 4 and 5). These results are in line with findings reporting the activation of rat astrocytes induced by cholesterol exposure *in vitro*, resulting in enhanced APP/BACE-1 interaction within lipid-rafts, increased APP content, and enhanced ROS production [39]. Moreover, recent observations from a single cell brain atlas of human AD indicated the diversity of astrocytes in AD under the control of the transcription factor EB, a master regulator of lysosomal function, which initiated a regulatory cascade containing multiple AD GWAS genes [40]. Taken in consideration that subjects with DS display abnormal lipid metabolism from the embryonic stages [41] and that *SOD1*, *BACE-2*, *S100β* and *APP* genes are located at HSA21 [42], it is conceivable that subjects with HSA21 trisomy could have a basal cholesterol-mediated astrocyte activation. These findings along with the observed increased NPC1 expression in DS individuals (Figure 2) suggests that an enhanced hippocampal lysosomal cholesterol trafficking could result in increased mitochondrial cholesterol loading in hippocampal areas, possibly coinciding with signs of early AD-pathogenesis. Moreover, elevated astrogial-STARD1 expression in individuals with AD implies accumulation of mitochondrial cholesterol in activated astrocytes within CA1 independently of NPC1. Whether this outcome reflects that post-mortem samples from patients with AD represent a late stage of the disease masking the early intra-organelle cholesterol mobilization remains to be further investigated.

Finally, whether the increase in hippocampal $A\beta_{42}$ deposits reflects an impaired Aβ clearance by increased lysosomal cholesterol remains to be further confirmed in human neurodegeneration. Although the astrocyte-dependent lipidation of ApoE could contribute to the ability of glia to clear Aβ burden, this event does not seem to occur in ApoE4-carrying subjects [2], and defects in Aβ clearance have been detected in cerebrospinal fluid of >98% of LOAD cases [43], which may reflect defects in the endolysosomal/autophagy system in the early neuropathological stages of AD [44]. In line with this possibility, we have recently reported that elevated intracellular cholesterol levels in a hypercholesterolemic mouse model increased Aβ-induced autophagosome formation, but impaired the fusion with lysosomal vesicles causing deficient autophagy-dependent Aβ degradation [45]. Considering that DS might serve as a model for early AD [12], the observations of increased lysosomal cholesterol loading support the notion that abnormal cholesterol distribution in lysosomes can impact mitochondrial function through sustained mitochondrial cholesterol accumulation and Aβ clearance, emerging as an early event in AD pathogenesis.

In conclusion, this exploratory study in post-mortem brains from patients with AD and DS revealed increased mitochondrial and lysosomal cholesterol levels in hippocampus from patients with AD and DS, which correlate with higher expression of STARD1 and NPC1. Moreover, our findings indicate the ability of STARD1 expression to discriminate controls from AD in the general population and in subjects with DS and suggest that STARD1 could be a potential marker associated with early molecular events of AD pathology. Further studies with a higher number of human samples are needed to validate these findings. In addition, future research using mice with tissue-specific deletion of STARD1 are warranted to define its role in AD pathology.

MATERIALS AND METHODS

Human brain samples

Twenty-one cases from the Biobank of Hospital Clinic/IDIBAPS of Barcelona were collected following approval of the Clinical Research Ethics Committee of the Hospital Clinic of Barcelona (HCB/2015/0595).

Samples were scored by CERAD scale (A-C) and Braak stage (0-VI) and categorized as AD, DS, and control groups. For each group, demographic data as well as clinical and anatomopathological diagnosis are detailed in Table 1. Please find the BRISQ checklist in Supplementary Methods detailing the biospecimen samples collected from patients with AD and DS.

mRNA isolation and RT-qPCR

Total RNA was extracted from 150 mg of frozen cortex of human brains, using TRIzol reagent (Invitrogen), cleaned by RNeasy columns (Qiagen), and quantified through Nanodrop spectrophotometer (Thermo-Fisher Scientific). Real-time qPCR was performed using the iScript™ One-Step RT-PCR Kit with SYBR® Green (Bio-Rad) following the manufacturer's instructions. Briefly, 200 ng of total RNA were mixed with 300 µmol/l of specific primers for each gene assessed (Supplementary Table 3) in 1× reaction buffer at final volume of 10.5 µl. RT-qPCRs were performed in triplicate using a CFX380 Real-Time System (Bio-Rad) following the manufacturer's instructions. Gene expression values were normalized using actin as housekeeping gene.

Western blotting

Human frozen cortex (350 mg) were homogenized on ice in anti-proteases/anti-phosphatases (Complete/PhosSTOP, Roche) containing RIPA lysis buffer. Protein quantitation was assessed by BCA (Pierce) and samples (90 µg/lane) were resolved by 4-12% SDS-PAGE (Bio-Rad), electrotransferred to nitrocellulose membranes (Trans-Blot Turbo, Bio-Rad), followed by 5% BSA-blocking and incubation with primary antibodies (Supplementary Table 4) at 4°C overnight. After washing, membranes were incubated 1 hr at RT with the corresponding horseradish peroxidase-coupled secondary antibodies and visualized using the Pierce ECL Western Blotting Substrate (Thermo Scientific). Immunoblots images were captured using LAS4000 (GE Healthcare) and quantitation of the bands was performed by Image J free software (NIH).

Immunohistochemistry

Paraffin sections (5 µm) of hippocampus were processed according to the avidin–biotin–peroxidase staining method (Vectastain ABC kit; Vector Lab), as described previously [7] and detailed in Supplementary Methods.

Recombinant GST-PFO probe

To optimally assess the localization of cholesterol in hippocampal tissues, we generated a recombinant Perfringolysin O (PFO) fusioned with Glutathione-S-Transferase (GST-PFO), as described [46]. In brain tissues, PFO binds and detects cholesterol in membranes when its levels exceed 30% mol, while the fusion with GST allows PFO detection by immunofluorescence. The sequence to design the plasmid was DNA M36704 (NCBI database) corresponding to the gen of PFO in the *Clostridium perfringens* genome. Additionally, the signal peptide was eliminated from the PFO gen to enable the intracellular stance of the protein. The resulted sequence was synthesized into the plasmid pGEX 4T-1 (GenScript) between the *BamHI* and *SmaI* restriction sites. The plasmid was engineered to make a fusion protein with the GST tag. After bacterial production, protein extraction and purification, the GST-PFO probe was dialyzed, concentrated, quantified and stored at −80°C.

Immunofluorescence

Paraffin sections (5 µm) of hippocampus were dewaxed/rehydrated and treated for antigen retrieval as was described above for immunohistochemical analysis. Sections were permeabilized with 0.2% Triton X-100 in blocking buffer (5% goat serum + 1% BSA in PBS) during 10 min, followed by washing ×3 with PBS and incubation overnight at 4°C with primaries antibodies (Supplementary Table 4) into a dark-humid chamber, as described in detail in Supplementary Methods.

Image analysis

Detection and quantitation of immunoreactivity for $A\beta_{42}$, p-tau, NPC1, and STARD1 was performed from high-resolution scanned immunohistochemical images of hippocampus using the Image J Software after *Color Deconvolution* plug-in [47], as detailed in Supplementary Methods.

Statistics

Data are shown as mean ± S.E.M and statistical analysis performed with the GraphPad Prism-5 software (San Diego, CA). Due to the number of analysed samples (≤7 for each group), nonparametric tests were employed. Differences between AD, DS and control samples were analysed with Kruskall-Wallis test followed by Mann-Whitney *U*-test to analyze the differences between two groups. The Spearman's rank-correlation coefficient r_s was also determined when pertinent. Two-tailed p values <0.05 were considered statistically significant. ROC curves were generated and the area under ROC curves (AUC) was calculated to evaluate sensitivity and specificity of immunolabeling within hippocampal regions. ROC curves from control group were compared to AD or DS or AD+DS groups. The cut-off points on the ROC curves at which accuracy of disease detection was maximal were selected.

Additional visualization of the association between markers and subject status (i.e. control, AD, or DS) was performed through multivariate data analysis by PCA using JMP 9.0 software (SAS Institute Inc.). PCA show the data variability as the covariance of samples for each marker (descriptors) projected into a subspace made of orthogonal linear axis, so-called principal components.

Abbreviations

AD: Alzheimer´s disease; $A\beta_{42}$: beta amyloid peptide 42; DS: Down syndrome; EOAD: early-onset AD; LOAD: late-onset AD; mGSH: mitochondrial GSH; MAM: mitochondrial ER-associated membranes; MIM: mitochondrial inner membrane; NFTs: neurofibrillary tangles; NPC1: Niemann Pick type C1 protein; PCA: principal component analysis; PFO: recombinant perfringolysin; p-tau: phosphorylated tau; StARD1: steroidogenic acute regulatory protein.

AUTHOR CONTRIBUTIONS

All authors read and approved the final manuscript. F.A. and S.N. performed gene expression, WB and immunohistochemistry procedures. F.A., G.G. and F.C. synthesized GST-PFO and performed immuno-fluorescence. F.A., C.G-R and J.C. F-Ch analysed and discussed data and wrote the manuscript.

ACKNOWLEDGMENTS

We want to thank Dr. María Carmona from the Hospital de la Santa Creu y San Pau for critically reading the manuscript and valuable suggestions.

FUNDING

We acknowledge the support from grants SAF2014-57674R, SAF-2015-69944R, and SAF2017-85877R from Plan Nacional de I+D, by the CIBEREHD from the Instituto de Salud Carlos III, by AGAUR of the Generalitat de Catalunya SGR-2017-1112, and by the "ER stress-mitochondrial cholesterol axis in obesity-associated insulin resistance and comorbidities"-Ayudas FUNDACION BBVA, Spain. We also acknowledge support from the center grant P50AA011999 Southern California Research Center for ALPD and Cirrhosis funded by NIAAA/NIH and by the European Cooperation in Science and Technology (COST) ACTION CA17112 Prospective European Drug-Induced Liver Injury Network, and Red Nacional 2018-102799-T de Enfermedades Metabólicas y Cáncer.

CONFLICTS OF INTEREST

The authors declare there are no conflicts of interest.

REFERENCES

1. Bharadwaj P, Solomon T, Malajczuk CJ, Mancera RL, Howard M, Arrigan DW, Newsholme P, Martins RN. Role of the cell membrane interface in modulating production and uptake of Alzheimer's beta amyloid protein. Biochim Biophys Acta Biomembr. 2018. [Epub ahead of print]. https://doi.org/10.1016/j.bbamem.2018.03.015 PMID:29572033

2. Arenas F, Garcia-Ruiz C, Fernandez-Checa JC. Intracellular cholesterol trafficking and impact in neurodegeneration. Front Mol Neurosci. 2017; 10:382. https://doi.org/10.3389/fnmol.2017.00382 PMID:29204109

3. Kågedal K, Kim WS, Appelqvist H, Chan S, Cheng D, Agholme L, Barnham K, McCann H, Halliday G, Garner B. Increased expression of the lysosomal cholesterol transporter NPC1 in Alzheimer's disease. Biochim Biophys Acta. 2010; 1801:831–38. https://doi.org/10.1016/j.bbalip.2010.05.005 PMID:20497909

4. Elustondo P, Martin LA, Karten B. Mitochondrial cholesterol import. Biochim Biophys Acta Mol Cell Biol Lipids. 2017; 1862:90–101. https://doi.org/10.1016/j.bbalip.2016.08.012 PMID:27565112

5. Webber KM, Stocco DM, Casadesus G, Bowen RL, Atwood CS, Previll LA, Harris PL, Zhu X, Perry G, Smith MA. Steroidogenic acute regulatory protein (StAR): evidence of gonadotropin-induced steroidogenesis in Alzheimer disease. Mol Neurodegener. 2006; 1:14. https://doi.org/10.1186/1750-1326-1-14 PMID:17018137

6. Barbero-Camps E, Fernández A, Baulies A, Martinez L, Fernández-Checa JC, Colell A. Endoplasmic reticulum stress mediates amyloid β neurotoxicity via mitochondrial cholesterol trafficking. Am J Pathol. 2014; 184:2066–81. https://doi.org/10.1016/j.ajpath.2014.03.014 PMID:24815354

7. Barbero-Camps E, Fernández A, Martínez L, Fernández-Checa JC, Colell A. APP/PS1 mice overexpressing SREBP-2 exhibit combined Aβ accumulation and tau pathology underlying Alzheimer's disease. Hum Mol Genet. 2013; 22:3460–76. https://doi.org/10.1093/hmg/ddt201 PMID:23648430

8. Wiseman FK, Al-Janabi T, Hardy J, Karmiloff-Smith A,

Nizetic D, Tybulewicz VL, Fisher EM, Strydom A. A genetic cause of Alzheimer disease: mechanistic insights from Down syndrome. Nat Rev Neurosci. 2015; 16:564–74. https://doi.org/10.1038/nrn3983 PMID:26243569

9. Startin CM, Hamburg S, Hithersay R, Al-Janabi T, Mok KY, Hardy J, Strydom A, Strydom A, Fisher E, Nizetic D, Hardy J, Tybulewicz V, Karmiloff-Smith A, et al, and LonDownS Consortium. Cognitive markers of preclinical and prodromal Alzheimer's disease in Down syndrome. Alzheimers Dement. 2019; 15:245–57. https://doi.org/10.1016/j.jalz.2018.08.009 PMID:30503169

10. Jack CR Jr, Knopman DS, Jagust WJ, Petersen RC, Weiner MW, Aisen PS, Shaw LM, Vemuri P, Wiste HJ, Weigand SD, Lesnick TG, Pankratz VS, Donohue MC, Trojanowski JQ. Tracking pathophysiological processes in Alzheimer's disease: an updated hypothetical model of dynamic biomarkers. Lancet Neurol. 2013; 12:207–16. https://doi.org/10.1016/S1474-4422(12)70291-0 PMID:23332364

11. Portelius E, Soininen H, Andreasson U, Zetterberg H, Persson R, Karlsson G, Blennow K, Herukka SK, Mattsson N. Exploring Alzheimer molecular pathology in Down's syndrome cerebrospinal fluid. Neurodegener Dis. 2014; 14:98–106. https://doi.org/10.1159/000358800 PMID:24992945

12. Lott IT, Head E. Dementia in Down syndrome: unique insights for Alzheimer disease research. Nat Rev Neurol. 2019; 15:135–47. https://doi.org/10.1038/s41582-018-0132-6 PMID:30733618

13. Zigman WB, Schupf N, Jenkins EC, Urv TK, Tycko B, Silverman W. Cholesterol level, statin use and Alzheimer's disease in adults with Down syndrome. Neurosci Lett. 2007; 416:279–84. https://doi.org/10.1016/j.neulet.2007.02.023 PMID:17353095

14. Torres S, García-Ruiz CM, Fernandez-Checa JC. Mitochondrial cholesterol in Alzheimer's disease and Niemann Pick type C disease. Front Neurol. 2019; 10:1168. https://doi.org/10.3389/fneur.2019.01168 PMID:31787922

15. Braak H, Del Trecidi K. Neuroanatomy and pathology of sporadic Alzheimer's disease. Adv Anat Embryol Cell Biol. 2015; 215:1–162. https://doi.org/10.1007/978-3-319-12679-1_1 PMID:25920101

16. Frost GR, Li YM. The role of astrocytes in amyloid production and Alzheimer's disease. Open Biol. 2017; 7:7. https://doi.org/10.1098/rsob.170228 PMID:29237809

17. Heneka MT, Carson MJ, El Khoury J, Landreth GE, Brosseron F, Feinstein DL, Jacobs AH, Wyss-Coray T, Vitorica J, Ransohoff RM, Herrup K, Frautschy SA, Finsen B, et al. Neuroinflammation in Alzheimer's disease. Lancet Neurol. 2015; 14:388–405. https://doi.org/10.1016/S1474-4422(15)70016-5 PMID:25792098

18. Davidson YS, Robinson A, Prasher VP, Mann DM. The age of onset and evolution of Braak tangle stage and Thal amyloid pathology of Alzheimer's disease in individuals with Down syndrome. Acta Neuropathol Commun. 2018; 6:56. https://doi.org/10.1186/s40478-018-0559-4 PMID:29973279

19. Lebouvier T, Pasquier F, Buée L. Update on tauopathies. Curr Opin Neurol. 2017; 30:589–98. https://doi.org/10.1097/WCO.0000000000000502 PMID:28914736

20. Braak H, Thal DR, Ghebremedhin E, Del Tredici K. Stages of the pathologic process in Alzheimer disease: age categories from 1 to 100 years. J Neuropathol Exp Neurol. 2011; 70:960–69. https://doi.org/10.1097/NEN.0b013e318232a379 PMID:22002422

21. Braak H, Del Tredici K. The pathological process underlying Alzheimer's disease in individuals under thirty. Acta Neuropathol. 2011; 121:171–81. https://doi.org/10.1007/s00401-010-0789-4 PMID:21170538

22. McGuinness B, Passmore P. Can statins prevent or help treat Alzheimer's disease? J Alzheimers Dis. 2010; 20:925–33. https://doi.org/10.3233/JAD-2010-091570 PMID:20182019

23. Schultz BG, Patten DK, Berlau DJ. The role of statins in both cognitive impairment and protection against dementia: a tale of two mechanisms. Transl Neurodegener. 2018; 7:5. https://doi.org/10.1186/s40035-018-0110-3 PMID:29507718

24. Dubois B, Feldman HH, Jacova C, Hampel H, Molinuevo JL, Blennow K, DeKosky ST, Gauthier S, Selkoe D, Bateman R, Cappa S, Crutch S, Engelborghs S, et al. Advancing research diagnostic criteria for Alzheimer's disease: the IWG-2 criteria. Lancet Neurol. 2014; 13:614–29. https://doi.org/10.1016/S1474-4422(14)70090-0 PMID:24849862

25. Malnar M, Hecimovic S, Mattsson N, Zetterberg H.

Bidirectional links between Alzheimer's disease and Niemann-Pick type C disease. Neurobiol Dis. 2014; 72Pt A:37–47. https://doi.org/10.1016/j.nbd.2014.05.033 PMID:24907492

26. Arbor SC, LaFontaine M, Cumbay M. Amyloid-beta Alzheimer targets - protein processing, lipid rafts, and amyloid-beta pores. Yale J Biol Med. 2016; 89:5–21. PMID:27505013

27. Colin J, Gregory-Pauron L, Lanhers MC, Claudepierre T, Corbier C, Yen FT, Malaplate-Armand C, Oster T. Membrane raft domains and remodeling in aging brain. Biochimie. 2016; 130:178–87. https://doi.org/10.1016/j.biochi.2016.08.014 PMID:27594339

28. Barrett PJ, Song Y, Van Horn WD, Hustedt EJ, Schafer JM, Hadziselimovic A, Beel AJ, Sanders CR. The amyloid precursor protein has a flexible transmembrane domain and binds cholesterol. Science. 2012; 336:1168–71. https://doi.org/10.1126/science.1219988 PMID:22654059

29. Area-Gomez E, Schon EA. Mitochondria-associated ER membranes and Alzheimer disease. Curr Opin Genet Dev. 2016; 38:90–96. https://doi.org/10.1016/j.gde.2016.04.006 PMID:27235807

30. Area-Gomez E, Schon EA. On the pathogenesis of Alzheimer's disease: the MAM hypothesis. FASEB J. 2017; 31:864–67. https://doi.org/10.1096/fj.201601309 PMID:28246299

31. Rissman RA, Mobley WC. Implications for treatment: GABAA receptors in aging, Down syndrome and Alzheimer's disease. J Neurochem. 2011; 117:613–22. https://doi.org/10.1111/j.1471-4159.2011.07237.x PMID:21388375

32. Stocco DM, Zhao AH, Tu LN, Morohaku K, Selvaraj V. A brief history of the search for the protein(s) involved in the acute regulation of steroidogenesis. Mol Cell Endocrinol. 2017; 441:7–16. https://doi.org/10.1016/j.mce.2016.07.036 PMID:27484452

33. Fernández A, Llacuna L, Fernández-Checa JC, Colell A. Mitochondrial cholesterol loading exacerbates amyloid beta peptide-induced inflammation and neurotoxicity. J Neurosci. 2009; 29:6394–405. https://doi.org/10.1523/JNEUROSCI.4909-08.2009 PMID:19458211

34. Hoozemans JJ, van Haastert ES, Nijholt DA, Rozemuller AJ, Scheper W. Activation of the unfolded protein response is an early event in Alzheimer's and Parkinson's disease. Neurodegener Dis. 2012; 10:212–15. https://doi.org/10.1159/000334536 PMID:22302012

35. Rodríguez-Arellano JJ, Parpura V, Zorec R, Verkhratsky A. Astrocytes in physiological aging and Alzheimer's disease. Neuroscience. 2016; 323:170–82. https://doi.org/10.1016/j.neuroscience.2015.01.007 PMID:25595973

36. Balboa E, Castro J, Pinochet MJ, Cancino GI, Matías N, Sáez PJ, Martínez A, Álvarez AR, Garcia-Ruiz C, Fernandez-Checa JC, Zanlungo S. MLN64 induces mitochondrial dysfunction associated with increased mitochondrial cholesterol content. Redox Biol. 2017; 12:274–84. https://doi.org/10.1016/j.redox.2017.02.024 PMID:28282615

37. Kishida T, Kostetskii I, Zhang Z, Martinez F, Liu P, Walkley SU, Dwyer NK, Blanchette-Mackie EJ, Radice GL, Strauss JF 3rd. Targeted mutation of the MLN64 START domain causes only modest alterations in cellular sterol metabolism. J Biol Chem. 2004; 279:19276–85. https://doi.org/10.1074/jbc.M400717200 PMID:14963026

38. Rodriguez-Vieitez E, Saint-Aubert L, Carter SF, Almkvist O, Farid K, Schöll M, Chiotis K, Thordardottir S, Graff C, Wall A, Långström B, Nordberg A. Diverging longitudinal changes in astrocytosis and amyloid PET in autosomal dominant Alzheimer's disease. Brain. 2016; 139:922–36. https://doi.org/10.1093/brain/awv404 PMID:26813969

39. Avila-Muñoz E, Arias C. Cholesterol-induced astrocyte activation is associated with increased amyloid precursor protein expression and processing. Glia. 2015; 63:2010–22. https://doi.org/10.1002/glia.22874 PMID:26096015

40. Grubman A, Chew G, Ouyang JF, Sun G, Choo XY, McLean C, Simmons R, Buckberry S, Landin DV, Pflueger J, Lister R, Rackham OJ, Petretto E, Polo JM. A single cell brain atlas in human Alzheimer's disease. bioRxiv. 2019. https://doi.org/10.1101/628347

41. Adelekan T, Magge S, Shults J, Stallings V, Stettler N. Lipid profiles of children with Down syndrome compared with their siblings. Pediatrics. 2012; 129:e1382–87. https://doi.org/10.1542/peds.2011-1262 PMID:22585768

42. Zigman WB, Lott IT. Alzheimer's disease in Down syndrome: neurobiology and risk. Ment Retard Dev Disabil Res Rev. 2007; 13:237–46.

https://doi.org/10.1002/mrdd.20163 PMID:17910085

43. Mawuenyega KG, Sigurdson W, Ovod V, Munsell L, Kasten T, Morris JC, Yarasheski KE, Bateman RJ. Decreased clearance of CNS beta-amyloid in Alzheimer's disease. Science. 2010; 330:1774. https://doi.org/10.1126/science.1197623 PMID:21148344

44. Cataldo AM, Peterhoff CM, Troncoso JC, Gomez-Isla T, Hyman BT, Nixon RA. Endocytic pathway abnormalities precede amyloid beta deposition in sporadic Alzheimer's disease and Down syndrome: differential effects of APOE genotype and presenilin mutations. Am J Pathol. 2000; 157:277–86. https://doi.org/10.1016/S0002-9440(10)64538-5 PMID:10880397

45. Barbero-Camps E, Roca-Agujetas V, Bartolessis I, de Dios C, Fernández-Checa JC, Marí M, Morales A, Hartmann T, Colell A. Cholesterol impairs autophagy-mediated clearance of amyloid beta while promoting its secretion. Autophagy. 2018; 14:1129–54. https://doi.org/10.1080/15548627.2018.1438807 PMID:29862881

46. Kwiatkowska K, Marszałek-Sadowska E, Traczyk G, Koprowski P, Musielak M, Lugowska A, Kulma M, Grzelczyk A, Sobota A. Visualization of cholesterol deposits in lysosomes of Niemann-Pick type C fibroblasts using recombinant perfringolysin O. Orphanet J Rare Dis. 2014; 9:64. https://doi.org/10.1186/1750-1172-9-64 PMID:24775609

47. Ruifrok AC, Johnston DA. Quantification of histochemical staining by color deconvolution. Anal Quant Cytol Histol. 2001; 23:291–99. PMID:11531144

SUPPLEMENTARY MATERIALS

Supplementary Methods

Immunohistochemistry analysis

After paraffin sections were dewaxed and rehydrated, the antigen retrieval of hippocampus sections was performed using 99% formic acid (5 min at RT), following by heating-incubation (120°C for 20 min) with 10 mM Tris/1mM EDTA/0.05% Tween 20; pH 9.0. Endogenous peroxidase was blocked using 3% H_2O_2/methanol for 45 min. In a dark-humid chamber, blocking of sections was performed using Dako antibody diluent background reducing components (Dako) for 20 min, and treated with the Avidin/Biotin blocking kit from Vector Lab according to the manufacturer's instructions and incubated overnight (4°C) with antibodies against human Aβ, pathological phospho-tau (Ser202 and Thr205), NPC1, and StARD1 (Supplementary Table 2). Sections were then incubated (1 hr) with the corresponding biotinylated secondary antibodies diluted 1:200, followed by ABC staining for 30 min. The immunoreactivities were visualized with diaminobenzidine (DAB enhanced liquid substrate system, Sigma). Sections were counterstained with hematoxylin (Dako) and mounted with a coverslip. The final stained hippocampal sections were then scanned in a 43X resolution using Panoramic DESK digital slice scanner with Carl Zeiss objectives (3DHISTECH) and images of entire hippocampus regions where capture using Panoramic Viewer software (3DHISTECH).

Immunofluorescence analysis

Secondary antibodies (Thermofisher) were diluted 1:200 in 1% Goat Serum containing 0.05% Triton X-100 in PBS and incubated (1 hr at RT) with the mix of anti-rabbit Alexa fluor-532 (for StARD1 or NPC1), anti-mouse Alexa fluor-635 (for $A\beta_{42}$), and anti-rat Alexa fluor-488 (for GFAP). Finally, sections were incubated (10 min) with 20 mM Hoechst 33342 dye (Thermofisher), washed and incubated (5 min) with 0.1 % sudan black dye (Sigma) in 70% ethanol to block autofluorescence, followed by mounting using fluorescent mounting medium (Dako).

Human hippocampal cryopreserved 14 µm thin sections were fixed in 4% paraformaldehyde for 20 min. In a dark-humid chamber, the sections were permeabilized with 0.2% Triton X-100 in blocking buffer (5% goat serum + 1% BSA in PBS) for 2 hr. Then, slices were incubated (3 hr at 4°C) with the probe GST-PFO (20µg/ml) in 1% Goat Serum containing 0.05% Triton X-100 in PBS, followed by incubation overnight (4°C) with primaries antibodies (Supplementary Table 4). Secondary antibodies were diluted 1:200 in 1% Goat Serum containing 0.05% Triton X-100 in PBS and incubated for 90 min at RT with the mix of anti-rabbit Alexa fluor-647 (for Tom20 or Lamp1), anti-mouse Alexa fluor-532 (for GST) and anti-rat Alexa fluor-488 (for GFAP). After washing, slices were incubated 5 min in Sudan black 0.1% in 70% ethanol to minimize autofluorescence and mounted with prolong antifade mountant with Dapi (Dako).

Images for all samples were taken with a Leica TCS SP5 laser scanning confocal system with a 63X oil immersion objective APO CS numerical aperture 1.4 equipped with a DMI6000 inverted microscope.

Image analysis

Briefly, after background subtraction and filtering processes (median, radius 2.0), segmentation of immunoreactivities was performed by the combination of H-DAB vector matrix of *Color Deconvolution* plug-in [14] – which separate channels corresponding to 3 determined colors of hematoxylin-DAB stain – with the local standard threshold of the "*Colour-2*" (brown) resulted images. Immunoreactivities were then subjected to particle analysis for acquiring the percentage of immunolabeled area relative with the total area of the image.

Confocal images of immunoreactivities for GFAP, NPC1 and StARD1 from hippocampal paraffin sections were analysed by Image J Software. In 10 different images of each hippocampal region (CA1, CA2 or CA3), percentage of total NPC1 or StARD1 mass containing astrocytes (GFAP+) were analysed using the *Colocalization nBits n-images* plug-in (Confocal Microscopy Unit, Medicine Faculty, University of Barcelona), which highlights the colocalized points of two 32-bits images (Figure 4A). Two points are considered as colocalized if their respective intensities are strictly higher than the threshold of their channels and if their ratio of intensity is strictly higher than the ratio setting value, which have been defined at 50%. Colocalization index is calculated as the ratio of colocalized points between total threshold-passed intensity and relativized with control group.

On the other hand, similar to as been described above to paraffin sections, detection of cholesterol within lysosomes or mitochondria into astrocytes was performed in cryopreserved hippocampal sections and analysed by confocal imaging using Image J Software. Immunofluorescence images were submitted to background subtraction and filtering processes with Median filter set at 2.0 of radius. Then, 0.4 µm spaced consecutive

images were stacked at maximum intensity and segmented by threshold to select the area of astrocytes (GFAP+). All marks outside GFAP+ area were clean in the corresponding images for GST+ and Tom20+/Lamp1+. Resulted images were then analysed using the *Colocalization nBits n-images* plug-in (Confocal Microscopy Unit, Medicine Faculty, University of Barcelona) as is described above.

BRISQ checklist

Based on Moore et al, Cancer Cytopathol 2011; 119(2):92–101. https://doi.org/10.1002/cncy.20147.

Intracellular cholesterol accumulation associated with astrogliosis in postmortem brains from patients with AD and DS collected from from Biobank of Hospital Clinic (IDIBAPS) with the approval of the Clinical Research Ethics Committee of the Hospital Clinic of Barcelona (HCB/2015/0595).

Biospecimen type	**Brain sections**
Anatomical site	Cortex and Hippocampus
Disease status of patients	Alzheimer with or without Down Syndrome, Controls without neurological disease
Clinical characteristics of patients	Patients with Dementia
Vital State of patients	Postmortem
Clinical diagnosis of patients	Alzheimer dementia
Pathology diagnosis	CERAD B-C and Braak V-VI; detailed in Methods and in Table 1
Collection mechanism	Postmortem dissection
Type of stabilization	On ice
Type of long-term preservation	Formalin fixation, freezing
Constitution of preservative	10% neutral-buffered formalin
Storage temperature	−80 ºC, 20 to 25 ºC
Storage duration	5-10 years
Shipping temperature	−170 ºC to −190 ºC, 20 to 25 ºC
Composition assessment and selection	Brain sections used for anatomopathological diagnosis of Alzheimer

Supplementary Figures

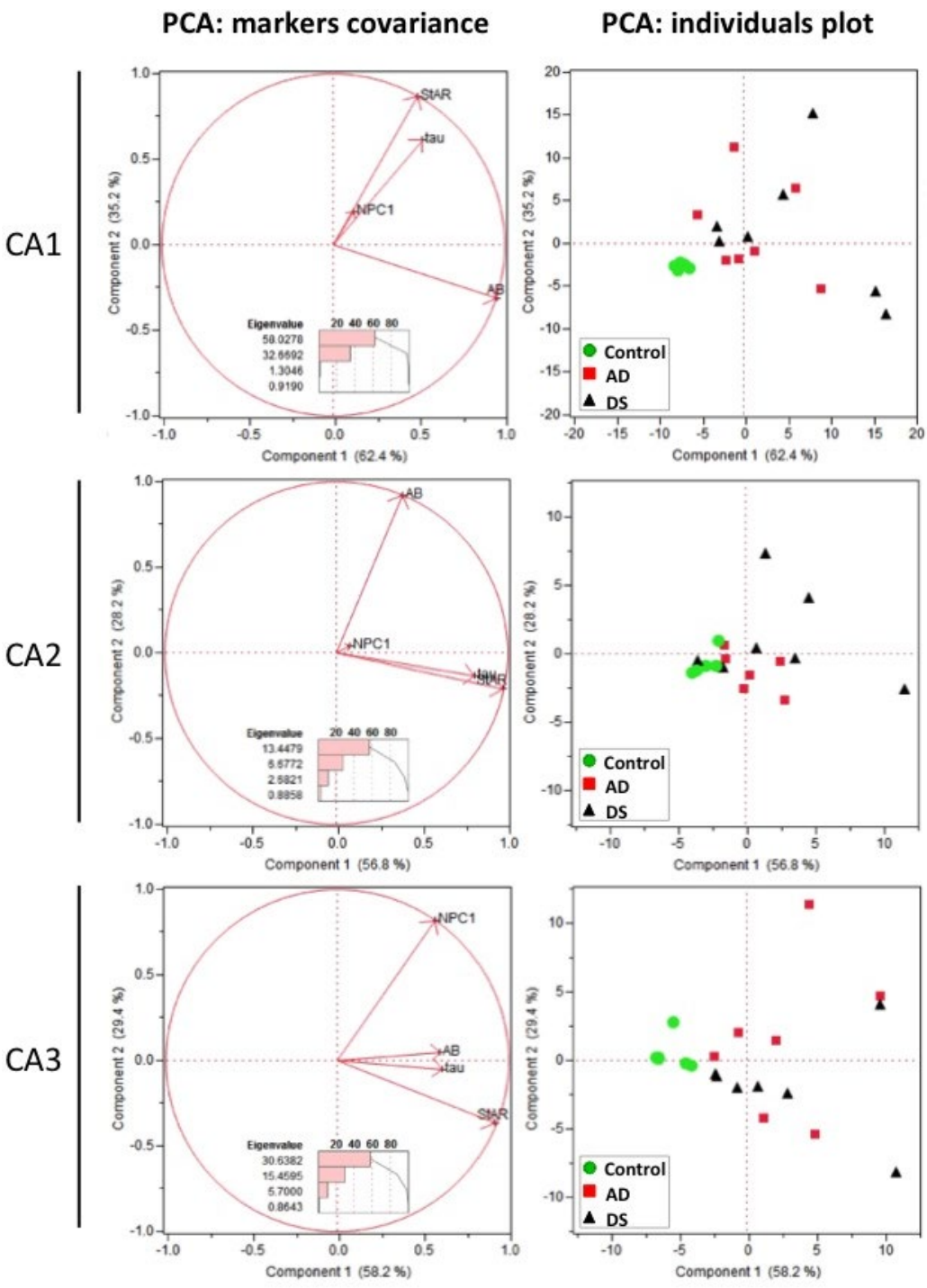

Supplementary Figure 1. Principal Component Analysis (PCA) of Aβ$_{42}$, p-tau, NPC1, and StARDl markers. For CA1, CA2, and CA3 hippocampus regions is show (left panel) the covariance between %area immunodetected by IHC of the corresponding marker, and the first principal plane (Component 1 + Component 2) represented on the first vectorial plan of the PCA. Histogram of Eigenvalues explain the variation. (Right panel) Distribution of AD, DS, and control samples onto the two first axes of the PCA.

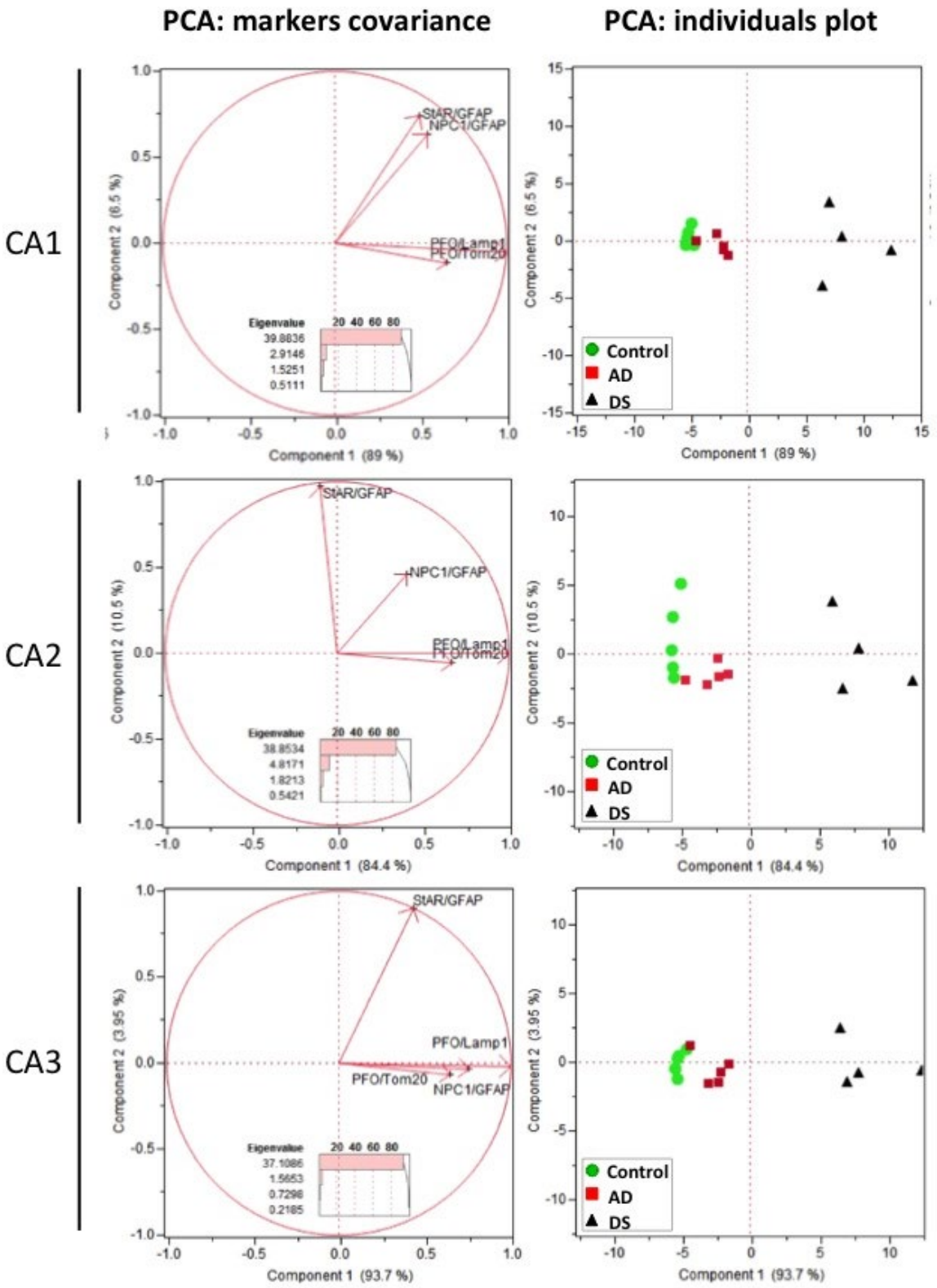

Supplementary Figure 2. Principal Component Analysis (PCA) of lysosomal and mitochondrial cholesterol contain and carriers within hippocampal astrocytes. (Left panel) First vectorial plan of the PCA that describe the covariance between descriptors (content of both glial cholesterol carriers and lysosomal/mitochondrial cholesterol content) and the first principal plane (Component 1 + Component 2). Histogram of Eigenvalues explain the variation. (Right panel) Distribution of AD, DS, and control samples onto the two first axes of the PCA.

Supplementary Tables

Supplementary Table 1. Overview of modulation of key proteins involved in intracellular cholesterol trafficking in the brain (1).

Control								
Cortical levels (n-fold) mean±SEM			Hippocampal levels (n-fold) mean±SEM					
			CA1		CA2		CA3	
Marker	mRNA	Protein[a]	Proteln[b]	GFAP+ colocalization	Proteln[b]	GFAP+ colocalization	Proteln[b]	GFAP+ colocalization
Aβ42	n.a.	n.a.	1.00 ± 0.262	n.a.	1.00 ±0.471	n.a.	1.00 ±0,323	n.a
p-tau	n.a.	n.a.	1.00 ±0.342	n.a.	1.00 ±0.368	n.a.	1.00 + 0.288	n.a.
NPC1	1.00 ±0.019	1.00 ± 0.017	1.00 ±0.173	1.00 ±0.196	1.00 ±0.357	1.00 ±0.120	1.00 ± 0.331	1.00 ±0.192
StARDl	1.00 ±0.015	1.00 ± 0.044	1.00 ±0.321	1.00 ±0.271	1.00 ±0.458	1.00 ±0.331	1.00 ±0.396	1.00 ±0.178
StARD3/ MLN64	1.00 ±0.030	1.00 ± 0.237	n.a.	n.a.	n.a.	n.a.	n.a.	n.a.
StARD4	1.00 ±0.023	n.a.	n.a.	n.a.	n.a.	n.a.	n.a.	n.a.
INSIG	n.a.	1.00 ± 0.053	n.a.	n.a.	n.a.	n.a.	n.a.	n.a.
SREBP2	n.a.	1.00 ± 0.028	n.a.	n.a.	n.a.	n.a.	n.a.	n.a.
Alzheimer´s disease								
Cortical levels (n-fold) mean±SEM			Hippocampal levels (n-fold) mean±SEM					
			CA1		CA2		CA3	
Marker	mRNA	Protein[a]	Proteln[b]	GFAP+ colocalization	Proteln[b]	GFAP+ colocalization	Proteln[b]	GFAP+ colocalization
Aβ42	n.a.	n.a.	7.04 ± 2.106	n.a.	1.97 ±0.727	n.a.	1.91 ±0.556	n.a.
p-tau	n.a.	n.a,	2.42 ±0.736	n.a.	1.63 ±0.554	n.a.	1.67 ±0.621	n.a.
NPC1	1.02 ±0.039	1.12 ±0.025 p_1=0.0043	8.07 ± 1.834 p_1=0.0006	0.92 ±0.194	3.77 ±0.800 p_1=0.0111	1.25 ±0.238	8.06 ± 1.539 p_1=0.0006	1.08 ± 0.087 p_2=0.0023
StARDl	1.00 ±0.014	1.25 ±0.056 P_1=0.0087	2.31 ±0.419 p_1=0.0379	2.60 ±0.563 P_1=0.0111	2.00 ±0.918	0.67 ± 0.232	5.92 ± 2.171 P_1=0.0047; p_2=0.0130	1.19 ±0.249
StARD3/ MLN64	0.99 ± 0.062	0.64 ± 0.150	n.a.	n.a.	n.a.	n.a.	n.a.	n.a.
StARD4	1.00 ±0.020	n.a,	n.a.	n.a.	n.a.	n.a.	n.a.	n.a.
INSIG	n.a.	1.05 ± 0.160	n.a.	n.a.	n.a.	n.a.	n.a.	n.a.
SREBP2	n.a.	1.12 ±0.161	n.a.	n.a.	n.a.	n.a.	n.a.	n.a.
Down syndrome								
Cortical levels (n-fold) mean±SEM			Hippocampal levels (n-fold) mean±SEM					
			CA1		CA2		CA3	
Marker	mRNA	Protein[a]	Proteln[b]	GFAP+ colocalization	Proteln[b]	GFAP+ colocalization	Proteln[b]	GFAP+ colocalization
A(342	n.a.	n.a.	11.30 ±3.423 Pi=0.0012	n.a.	4.27 ±1.275 Pi=0.0177	n.a.	3.99 ± 1.051 Pi=0.0221	n.a.
p-tau	n.a.	n.a.	2.59 ±0.783	n.a.	2.29 ±0.784	n.a.	2.88 ± 1.135	n.a.
IMPCl	1.08 ±0.028	1.04 ±0.036	9.86 ±2.413 p_1=0.0006	1.62 ±0.420	5.41 ±1.740 P_1=0.0111	2.05 ± 0.577	8.79 ±1.822 P_1=0.0006	1.08 ± 0.087 p_1=0.0023
StARDl	1.08 ±0.013 P_1=0,0087	1.35 ±0.044 P_1=0.0043; p_2=0.0159	0.97 ±0.182 p_2=0.0111	2.81 ± 0.755	0.56 ±0.212	0.80 ± 0.246	2.62 ±1.290 p_2=0.0130	2.01 ±0.311 P_1=0.0111
StARD3/ MLN64	1.13 ±0.053	1.47 ±0.277	n.a.	n.a.	n.a.	n.a.	n.a.	n.a.

StARD4	1.03 ± 0.008	n.a.	n.a.	n.a.	n.a.	n.a.	n.a.	n.a.
INSIG	n.a.	1.14 ±0.043	n.a.	n.a.	n.a.	n.a.	n.a.	
SREBP2	n.a.	1.14 ±0.061	n.a.	n.a.	n.a.	n.a.	n.a.	n.a.

NOTE: P values are calculated by differences against control (pi) or differences between AD and DS (pz).

Supplementary Table 2. Overview of modulation of key proteins involved in intracellular cholesterol trafficking in the brain (1).

	Astrocyte (GFAP+) cholesterol (PFO+) colocalization (n-fold)		
Organelle marker	**Control**	**AD**	**DS**
Tom20 (mitochondria)	1.00 ±0.257	2.55 ± 0.297; p_1=0.0079	2.77 ± 0.203; p_1=0.0159
Lampl (lysosome)	1.00 ±0.136	3.43 ± 0.502; p_1=0.0079	14.41 ± 1.322; $p_{1,2}$=0.0079

Supplementary Table 3. Oligonucleotides used for gene expression analysis by RT-qPCR.

Gene	Sequence
StARD1	5′-GAGGAGGCCATGCAGAA
	5′-GAACACCTTGCCCACATC
StARD3	5′-AGTGAGGAGCCCAGGGAG
	5′-CCGTGGCTGACATGGAG
StARD4	5′-CGTTTTCTTAGCAACTCGCC
	5′-CTTCCACGTCCTTGCTTCAC
NPC1	5′-CATCCTTTGGCAATGGTTTT
	5′-CTGCTGCTACTGTGTCCAGC
β-Actin	5′-TTGCCGACAGGATGCAGAA
	5′-GCCGATCCACACGGAGTACT

Supplementary Table 4. Primary antibodies used in this study.

Antibody	Source and type	Company	WB dilution	IHC/IF dilution
StARD1	Rabbit monoclonal	Abcam (ab133657)	1:1000	1:200
StARD3 (MLN64)	Rabbit polyclonal	Sant Cruz (sc-292868)	1:1000	
SREBP2	Rabbit polyclonal	Abcam (ab28482)	1:500	
INSIG-1	Rabbit polyclonal	Abcam (ab70784)	1:1000	
NPC-1	Rabbit polyclonal	Abcam (ab36983)	1:500	1:200
Aβ human (6F/3D)	Mouse monoclonal	Dako (M0872)		1:2000
Lamp1	Rabbit polyclonal	Sant Cruz (sc-5570)		1:200
Tom20	Rabbit polyclonal	Sant Cruz (sc-11415)		1:200
GFAP	Rat monoclonal	Calbiochem (345860)		1:200
Glutathione-S-Transferase (GST)	Mouse monoclonal	Sant Cruz (sc-374171)		1:200
PHF-tau (AT8)	Mouse monoclonal	Thermofisher (MN1020)		1:200
β-Actin-HRP	Mouse monoclonal	Sigma (A3854)	1:20000	
NeuN	Mouse monoclonal	Millipore (MAB377)		1:200
IBA1	Mouse monoclonal	Santa Cruz (sc-32725)		1:200